Machining of a Zr–Ti–Al–Cu–Ni metallic glass

Mustafa Bakkal [a], Albert J. Shih [b], Ronald O. Scattergood [c,*], C.T. Liu [d]

[a] *Department of Mechanical and Aerospace Engineering, NC State University, Raleigh, NC 27695, USA*
[b] *Department of Mechanical Engineering, University of Michigan, Ann Arbor, MI 48109, USA*
[c] *Department of Materials Science and Engineering, NC State University, Campus Box 7907, Raleigh, NC 276957907, USA*
[d] *Oak Ridge National Lab, Oak Ridge, TN 37831, USA*

Abstract

$Zr_{52.5}Ti_5Cu_{17.9}Ni_{14.6}Al_{10}$ metallic glass machining chips were characterized using SEM, X-ray diffraction and nano-indentation. Above a threshold cutting speed, oxidation of the Zr produces high flash temperatures and causes crystallization. The chip morphology was unique and showed the presence of shear bands, void formation and viscous flow.
© 2003 Acta Materialia Inc. Published by Elsevier Ltd. All rights reserved.

1. Introduction

Bulk metallic glass (BMG) alloys are metal alloys with no long-range atomic order. A variety of rapid solidification techniques are used to produce BMG. These materials can exhibit unique mechanical, magnetic, and corrosion properties. Although casting is the most commonly used method for mass-producing BMG components, machining can be an important process for the manufacture of BMG parts with stringent dimensional accuracy and surface roughness requirements. The work-material in machining is subject to high temperature and strain-rate deformation conditions, for example, strain rates up to 10^5 s^{-1} and heating rates over 10^5 K s^{-1} can occur during chip formation [1]. Machining is therefore a simple method to investigate the response of BMG under extreme deformation conditions. This research studies lathe-turning of the BMG $Zr_{52.5}Ti_5Cu_{17.9}Ni_{14.6}Al_{10}$ [2,3].

One of the relevant properties of the BMG is its very low thermal conductivity, 4 W/m K [4], which is even lower than the 6–7 W/m K of Ti alloys. This can lead to the generation of high temperatures in machining chips. For example, during the machining of Ti alloys adiabatic shear localization causes serrated chip formation [5–7]. A novel feature observed during machining of the BMG at higher cutting speeds was the emission of bright light from the tool-workpiece contact area. Light emission has been observed during fracture of the same BMG by previous investigators [3,8,9].

2. Experimental procedure

The machining tests were conducted on an EMCO PC Turn 125 computer-controlled (CNC) lathe using a TiN coated WC-Co insert (Seco CCMT 09T304) with a 0.4 mm tip radius and a 5° rake angle. All tests were conducted dry without using coolant. Turning tests were done at 0.025 mm feed/rev, 0.5 mm depth of cut, and three cutting speeds, 0.38, 0.76, and 1.52 m/s, using a 6.35 mm diameter as-cast BMG rod. The depth of cut and feed/rev were kept constant so that the uncut chip profile was the same for all cutting speeds, as is shown in Fig. 1(a). Chip temperature measurements were made using an Ocean Optics USB2000 infrared spectrometer with a 0.72–0.98 μm wavelength range. Details of the temperature measurement technique have been described previously [10]. Machining chips were collected and mounted in epoxy molds for field-gun emission SEM analysis. The molded samples were cut and lapped to generate cross-sections of the chip. During molding, the chip was carefully positioned so that the plane of the polished cross-section coincided with the plane

---

*Corresponding author. Tel.: +1-919-515-7843; fax: +1-919-515-7724.
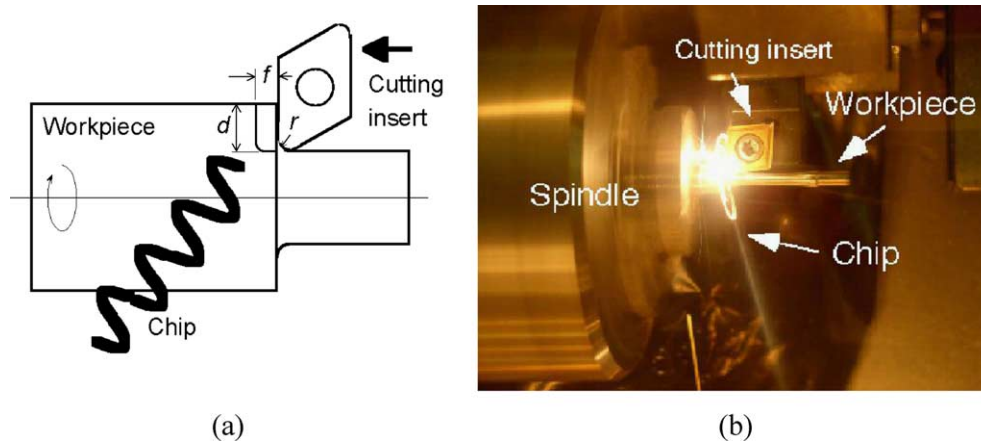*E-mail address:* ron_scattergood@ncsu.edu (R.O. Scattergood).

Fig. 1. (a) Schematic for lathe turning. The chip profile is unchanged when the depth-of-cut d, feed/rev f, and tip radius r, are fixed. (b) Light emission from tool-workpiece contact area and chip for a cutting speed of 1.52 m/s.

containing the surface normal and chip-flow direction (orthogonal-cutting view). A Scintag X-ray diffractometer with copper radiation and a liquid N_2-cooled Ge detector was used for the diffraction analysis of the chips and the machined surfaces. Nano-indentation tests were conducted using a MTS Nano-indenter™ II fitted with a Berkovich diamond indenter.

3. Results and discussion

The emission of light at the two highest cutting speeds, 0.76 and 1.52 m/s, was observed during machining of the BMG. As shown in Fig. 1(b), the tool-workpiece contact region emits very bright light once it exceeds a threshold temperature at higher cutting speeds. The chip remains glowing as a "light string" and the light emission decays along the chip length after leaving the contact region. No light emission was observed while machining at the lowest cutting speed, 0.38 m/s. Light emission using the same BMG was reported by Gilbert et al. [8], Liu et al. [3], and Horton [9] for fast fracture. Gilbert et al. [8] measured flash temperatures of ∼3175 K in air and ∼1400 K in nitrogen on the fracture surfaces of the BMG. They suggested that this was due to oxidation of fresh material exposed during rupture. Flash temperature measurements were made during machining in air in this study using an infrared spectrometer method [10]. The measured flash temperatures were ∼2700 K at the two highest cutting speeds. Within the uncertainty of the temperature measurement, this agrees with the previous results for fracture-induced light emission in air. Chip temperatures could not be measured at the lowest cutting speed because the radiation intensity was too low for the spectrometer method.

Deformation of metallic glass is, in general, very inhomogeneous with the occurrence of localized shear bands. In tensile tests, and often in unconstrained compression tests, the BMG fails catastrophically due to propagation of through-section shear bands [3]. This results in essentially no macroscopic plastic strain, analogous to brittle materials. Nevertheless, the Zr-based metallic glasses are reported to have fracture toughness values exceeding 50 MPa m$^{1/2}$ [3,11], comparable to ductile engineering metals. For the constrained deformation conditions operative during machining, catastrophic fracture does not occur and the BMG produces a continuous ductile chip resembling that found for conventional metal machining. This response is consistent with the high fracture toughness.

Deformation morphology in the BMG machining chips was characterized using SEM. Some chips were collected and observed in the SEM without further preparation. Fig. 2 shows micrographs at three magnification levels for these chips at the three cutting speeds. For the two lower cutting speeds, 0.38 and 0.76 m/s, shown in Fig. 2(a) and (b), large shear lamella occur, somewhat similar to the serrated chips produced using Ti alloys [6,7]. Thin, localized shear bands exist between the lamella. No consistent chip twist or curl occurs, in contrast to chips formed during machining of conventional metals. At the highest cutting speed, 1.52 m/s, shown in Fig. 2(c), chip formation is a combination of irregular lamellar segments in the midsection, surrounded by string-like features resembling "taffy-pulls". This is clearly different from the chip morphology at lower cutting speeds, and is unique for metal machining.

Examination of the chip morphology in Fig. 2 suggests that temperature-induced changes in the deformation response occur as the cutting speed increases. At higher cutting speeds, the temperature in the chip-separation zone will increase and can be concentrated further by adiabatic shear band formation. Temperatures above the glass transition, T_g, will promote viscous flow during deformation. The machining temperature must be high enough to counteract an upward shift in T_g due
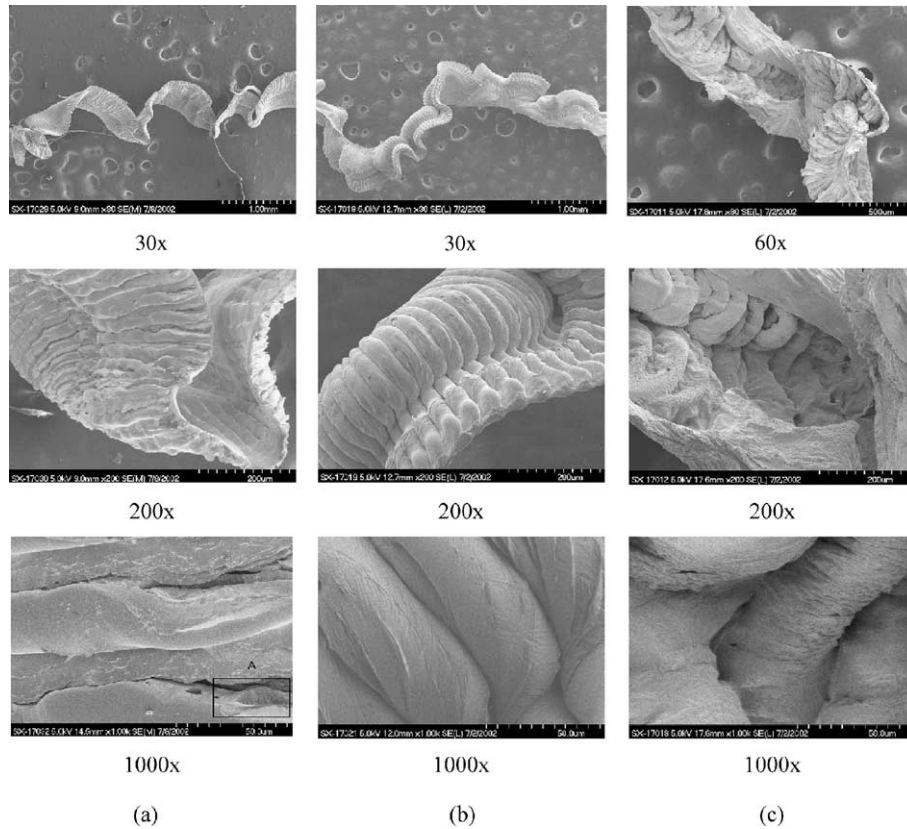
Fig. 2. SEM micrographs of chips at the (relative) magnification scales indicated. Cutting speeds: (a) 0.38 m/s. (b) 0.76 m/s. (c) 1.52 m/s.

to the very high strain rates that occur in machining. At the 0.38 m/s cutting speed, Fig. 2(a) shows that crack-like separations occur between the shear lamella. No such crack-like features can be seen between lamella generated at the 0.76 m/s cutting speed, shown in Fig. 2(b). Fig. 2(c) shows the presence of extensive viscous flow at the 1.52 m/s cutting speed.

Void formation occurred in the shear zones between lamella at the lowest cutting speed. The area (inset A at 1000×) shown in Fig. 2(a) is shown at higher magnification in Fig. 3. Voids on the order of 0.5–2 μm in diameter are found. Void formation was not observed in the shear zones for the higher cutting speeds. A local increase in free volume due to void creation, typically in the form of veinal patterns along fracture surfaces, has been observed as a primary mechanism for localized shear deformation in BMG subjected to uniaxial deformation [12,13]. Such features do not change significantly for Zr-based BMG deformed at very high strain rates using Hopkinson bar tests [13]. The BMG deformation mode can be characterized as elastic response followed by catastrophic fracture propagated by localized shear bands. The lack of voids present in the shear zones for chips cut at the higher cutting speeds suggests that the elastic strain that triggers intense localized shear may be less effective. Since chip temperatures are dramatically increased at the higher speeds, the onset of global viscous flow in the chips would reduce elastic driving forces, thereby modifying or inhibiting a free-volume shear mechanism. This appears consistent with the chip morphology seen in Fig. 2.

Optical microscopy was done on etched cross-sections of the chips as a preliminary step to characterize changes in the microstructure due to machining. Features that suggested the presence of a surface layer and interior crystallization were found for chips produced at the higher cutting speeds, 0.76 and 1.52 m/s. No such
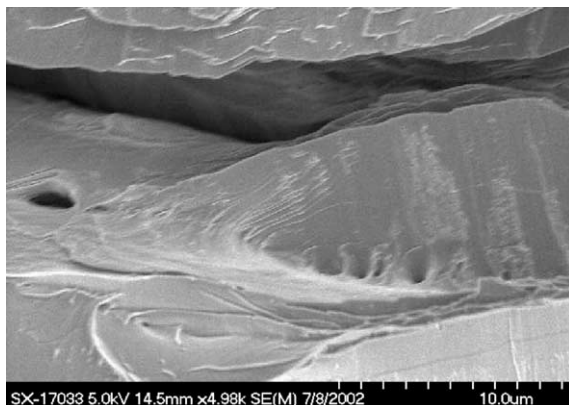

Fig. 3. Close-up view of inset A in Fig. 2(a) (bottom frame).

features could be found for the lowest cutting speed. Field-gun emission SEM observations were made on un-etched cross-sections of the chips to better reveal the internal structural details. SEM micrographs of a chip cross-section for a 1.52 m/s cutting speed are shown in Figs. 4 and 5. In general, three regions can be distinguished by adjusting the contrast conditions in the SEM. A surface layer marked by O, presumably due to oxidation driven by the high flash temperature, surrounds the chip in Fig. 4. Different grayscale contrast regions seen in Fig. 5 are visible within the interior of the chip. Because of the change in the SEM settings, the surface O layer in Fig. 4 is not visible in Fig. 5. The dark leaf-like regions near the surface in Fig. 5(a) and (b) represent one variant of a crystallized phase. The interior region shown at higher magnification in Fig. 5(c) displays a eutectic-like crystalline structure. The amount of crystallization varied somewhat for different chip cross-sections, but was near 100% in most cases. Similar structural features occurred for the chips produced at 0.76 m/s, but the overall amount of crystallization was not as extensive as that for 1.52 m/s.

Energy dispersive spectroscopy (EDS) analysis and backscatter Kikuchi diffraction (EBSD) analysis was done as part of the SEM characterization. These results showed that the different grayscale regions in Fig. 5 have different chemical contents, and are indeed crystalline phases. However, further identification of the crystal structures and chemical compositions was beyond the scope of the present study. The crystallization of $Zr_{52.5}Ti_5Cu_{17.9}Ni_{14.6}Al_{10}$ was investigated by Wang et al. [14]. Tetragonal Zr_2Ni and hexagonal [Ni,(Zr,Ti)] form as equilibrium phases under N_2 atmosphere. However under the extreme heating, oxidation and cooling conditions imposed during machining, non-equilibrium phases could be present in the chips. A more comprehensive investigation of the crystallization products

Fig. 5. SEM micrograph of a cross-section of a chip cut at 1.52 m/s. (a) 400×, (b) 1000×, (c) 2000×. Contrast is due to back-scattered secondary electrons (BSE).

formed during machining is being done using SEM and TEM, and will be reported elsewhere [15].

X-ray diffraction was done on collected chips (not cross-sectioned) and machined surfaces. Fig. 6(a)–(c) show the broad diffraction peaks that were obtained for the as-received BMG, the machined surfaces at all cutting speeds and the chips produced at the lowest cutting speed, 0.38 m/s. The broad peak represents the fully amorphous glass phase, as was reported by Liu et al. [3] and Wang et al. [14]. At the higher cutting speeds, 0.76 and 1.52 m/s, the diffraction pattern obtained from the chips is shown in Fig. 6(d) and (e). The peak positions match exactly those for ZrO_2. Several additional weak diffraction peaks are also present, but these could not be matched conclusively with any of the expected tetrago-
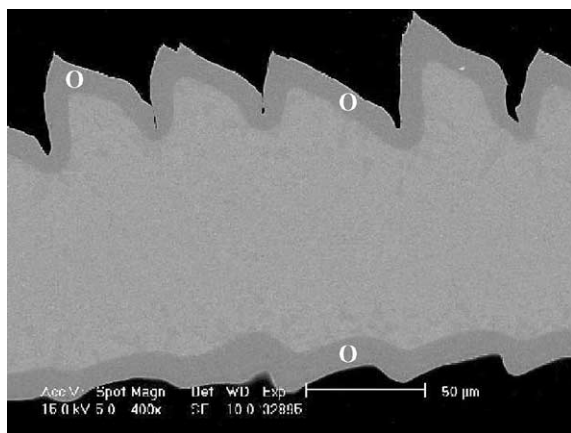

Fig. 4. SEM micrograph of a cross-section of a chip cut at 1.52 m/s. An oxide layer (O) surrounds the chip. Contrast is due to secondary electrons (SE).
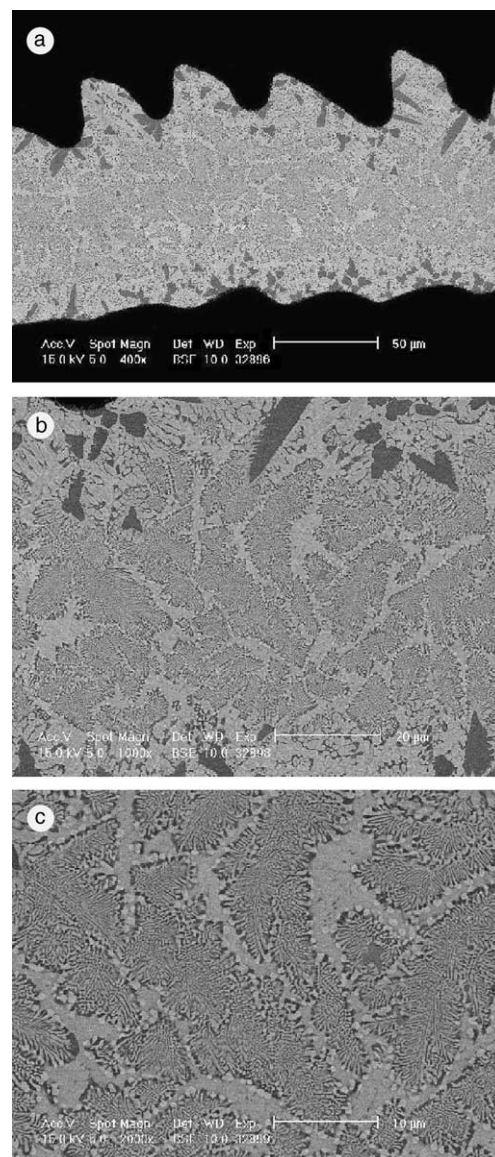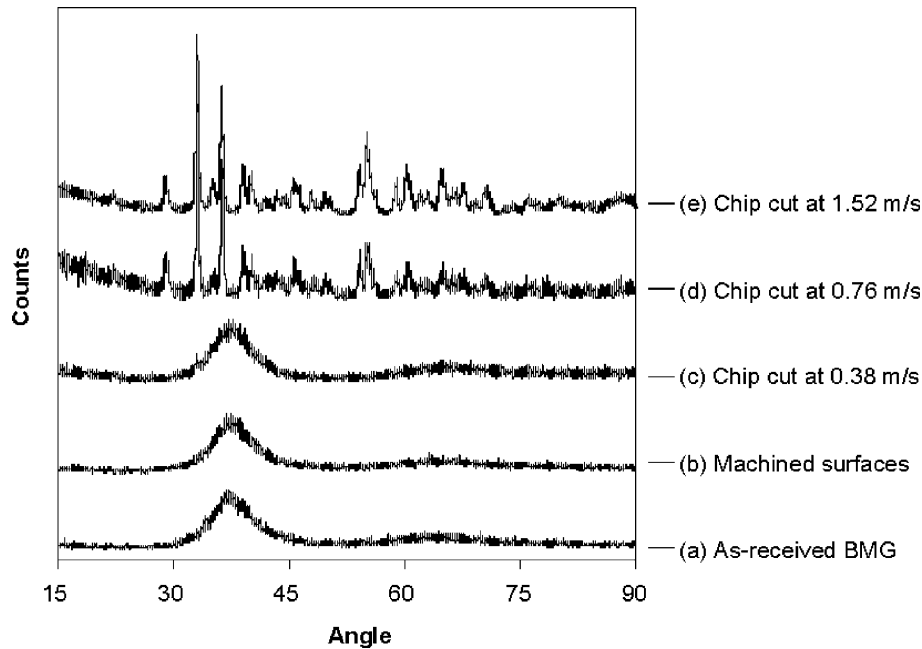
Fig. 6. Relative X-ray intensity vs. diffraction angle (2θ) for the cases indicated.

nal or hexagonal crystalline phases for the BMG. The X-ray data confirms the presence of an oxide layer on the chips cut at the higher speeds, and indicates that Zr undergoes the highly exothermic oxidation reaction that leads to the light emission shown in Fig. 1(b). The fact that crystalline phases revealed by SEM in Fig. 5 could not be detected using X-ray diffraction can be attributed to the absorption of the incident and diffracted X-rays by the overlying oxide layer. A simple calculation shows that a ZrO_2 oxide layer thickness on the order of 10–15 μm, as seen in Fig. 4, will reduce the diffracted X-ray intensity from the interior region of the chips by at least 90–95%. In contrast to the chips, the machined surfaces do not undergo crystallization at any of the cutting speeds This can be attributed to the fact that surfaces remain cooler with a very low thermal conductivity material like the BMG because a major portion of the heat generated will flow into the chips [16].

Nano-indentation tests were performed across the polished cross-sections of chips produced at the lowest and highest cutting speeds, 0.38 and 1.52 m/s. Fifty indents were made across each section. Results for the average hardness and elastic modulus are summarized in Table 1. Significant increases in hardness and elastic modulus are found for the highest cutting speed. These

changes are consistent with the differences observed between the amorphous and crystallized BMG [14].

4. Summary and conclusions

Machining of the BMG, $Zr_{52.5}Ti_5Cu_{17.9}Ni_{14.6}Al_{10}$, produces ductile chip removal, consistent with its reported high fracture toughness. Above a threshold cutting speed, the low thermal conductivity leads to chip temperatures high enough to cause oxidation of the Zr. The exothermic reaction produces flash temperatures on the order of 2700 K, accompanied by intense light emission. The high temperature produced by this reaction causes crystallization within the chips. The chip morphology shows pronounced shear lamella separated by regions of shear localization. As the cutting speed increases, the morphology suggests that increasing amounts of viscous flow control the chip-removal process. Finally, it is noteworthy that viscous flow and crystallization can occur during the machining of the bulk metallic glass, even though the heating/cooling rates and strain rates will be very high.

Acknowledgements

Table 1
Nano-indentation test results

Cutting speed (m/s)	Average hardness (GPa)	Average elastic modulus (GPa)
0.38	6.05	93.13
1.52	9.40	140.5

References

[1] Shih AJ. Int J Mach Tools Manufact 1996;36:255.

[2] Lin XH, Johnson WL, Rimm WK. Mater Trans, JIM 1997;38:473.

[3] Liu CT, Heatherly DS, Easton CA, Carmichael JH, Schneibel JH, Chen CH, et al. Metall Mater Trans A 1998;29A:1811.

[4] Ustundag E, Clausen B, Hanan JC, Bourke MAM, Winholtz A, Peker A. Mater Res Soc Symp Proc 1999;554:431.

[5] Recht RF. J Appl Mech 1964;31:189.

[6] Komanduri R, Brown RH. J Eng Indus 1981;103:33.

[7] Sheikh-Ahmad J, Bailey JA. J Manufact Sci Eng 1997;119:307.

[8] Gilbert CJ, Ager JW, Schroeder V, Ritchie RO, Lloyd JP, Graham JR. Appl Phys Lett 1999;74:3809.

[9] Horton JA, Wright JL, Schneibel JH. Mater Res Soc Symp Proc 1999;554:185.

[10] Curry AC, Shih AJ, Scattergood RO, Kong J, McSpadden SB. J Am Ceram Soc 2003;86:333.

[11] Gilbert CJ, Ritchie RO, Johnson WL. Appl Phys Lett 1997;71:476.

[12] Wright WJ, Saha R, Nix WD. Mater Trans 2001;42:642.

[13] Subhash G, Dowding RJ, Kecskes LJ. Mater Sci Eng A 2002;334:33.

[14] Wang JG, Choi BW, Nieh TG, Liu CT. J Mater Res 2000;13:798.

[15] Bakkal M, Liu CT, Watkins TR, Scattergood RO, Shih AJ. Intermetallics, 2003, in press.

[16] Swinehart HJ. Cutting tool material selection. Dearborn: American Society of Tool and Manufacturing Engineers; 1968. p. 13.